EISSN: 2707-0425

East African Journal of Science, Technology and Innovation, Vol. 3 (3): June 2022

Effect of Thickness and Deposition Angle on Optical Transmittance of ZnS/Ag Nanostructures

[1]BWAYO E., [1]IREETA T W., [1]MUKIIBI D., [1]OKULLO W., [1]OKELLO D., [1]LUGOLOLE R*

[1*] Department of Physics, School of Physical Sciences, College of Natural Sciences, Makerere University, Uganda.

* Correspondence: bwayoedward@gmail.com

Abstract

This paper presents the optical transmittance properties of thermally evaporated coatings of ZnS/Ag nanostructures as a function of film thickness and deposition angle designed to mitigate the challenges of indoor heating and their effects on low temperature storage facilities. The nanostructures were deposited on glass by varying the film thickness and deposition angle of both silver and zinc sulphide nanofilms at a pressure of 2.5×10^{-5} mBars in the diffusion pump microprocessor vacuum coater (Edwards AUTO 306). The optical transmittance of the coatings was measured at normal incidence in the wavelength range of 250-2500 nm of the incident electromagnetic radiation. Spectral studies showed that the transmittance decreased with increase in the film thickness of the ZnS/Ag nanostructures and the optical transmittance increased with increase in deposition angle of zinc sulphide in the infrared region. The transmittance of (4 nm)ZnS/Ag, (7 nm)ZnS/Ag, (10 nm)ZnS/Ag and (15 nm)ZnS/Ag samples deposited at normal angle in the visible region had peaks at 61.7%, 66.3%, 54.9%, and 18.0% respectively. The transmittance of the nanostructures increased with the increase in deposition angle of silver nanoparticles. Thus optical transmittance measured at 1800 nm wavelengths for ZnS(0^o)/Ag(0^o), ZnS(0^o)/Ag(30^o) and ZnS(0^o)/Ag(60^o) were 2.8%, 21.7% and 22.1% respectively. The coating of ZnS at high deposition angle decreased transmittance in the visible wavelength. The transmittance peak values in the visible region measured up to 51.1%, 53.5%, and 45.1% for (4 nm)ZnS(0^o)/Ag(0^o) and (4 nm)ZnS(0^o)/Ag(30^o) and (4 nm)ZnS(0^o)/Ag(60^o) samples respectively. However, increase in deposition angle of (10nm)ZnS/Ag nanostructures measured at 1000 nm; ZnS(0^o)/Ag(30^o), ZnS(30^o)/Ag(30^o) and ZnS(60^o)/Ag(30^o) increased transmittance in the infrared wavelengths from 9% to 12% and 34% respectively. Therefore, to increase transmittance in the visible region, the Zinc sulphide nanoparticles should be coated on silver at low deposition angles. However, the general observation that has been made was that, the oblique deposition of zinc sulphide had minimal impact on optical transmittance in the visible spectrum.

Keywords: *Nanostructures; deposition angle; film thickness; Transmittance; ZnS/Ag films*

Received: 09/12/21
Accepted: 13/06/22
Published: 30/06/22

Cite as: *Bwayo et al., (2022)* Effect of Thickness and Deposition Angle on Optical Transmittance of ZnS/Ag Nanostructures. *East African Journal of Science, Technology and Innovation 3(3).*

Introduction

Light energy from the Sun contains short wavelengths infrared radiation that conveys much of the heat energy into the earth's atmosphere (Wang *et al.,* 2021; Usami & Kawasaki, 2012). When the short wavelength infrared radiation enters into any building envelope, it leads to the accumulation of heat indoors that negatively affects the energy efficiency of storage facilities for medicines, pharmaceuticals, industrial processes as well as materials that are chemically stable at relatively low temperatures in addition to habitable human comfort. The thermal flux from the incident infrared radiation is the most outstanding problem which must be treated with due agency to address the challenges of indoor heating (Erell *et al.,* 2004; Kapsis & Athienitis, 2015). The application of ZnS/Ag nanostructured coatings on the outer surface of the glass window can be tailored to control the amount of solar radiation entering the building envelope.

The visible region of the electromagnetic spectrum contains about 75% - 89% of the short wavelength infrared radiation (Ha, 2016). This radiation when incident on the building may be reflected, transmitted and/or absorbed by the roof, walls and fenestration. Though several researches have been done to reduce thermal conductivity through walls and the roofs of buildings (Bwayo & Obwoya, 2014), thermal radiation transfer through the transparent windows and doors remains the biggest challenge in the indoor cooling and heating. A lot of effort has been devoted to improve energy efficiency by placing transparent materials such as polyethylene, depositing thin metal and/or dielectric films to modify the spectral characteristics such as the optical transmittance and absorbance of the visible and near infrared radiation. However, the deposition of thin metal or dielectric films on glass has been found to change greatly the spectral properties of glass (Hassouneh *et al.,* 2010; Wang *et al.,* 2016; Zahiri & Altan, 2016).

To modify the spectral characteristics of glass depends on several factors namely, deposition conditions (pressure, temperature, flux rate), deposition angle, film thickness including the deposition method (Macleod, 2010; Dalapati *et al.,* 2018). A suitable choice has to be made for the selection of materials including the film thickness, deposition angles to enhance the transmittance in the visible region and reduce transmittance in the near infrared region. Many elements notably copper, zinc, silver and other compounds of the transition elements have inherent properties that qualify them for use in transparent multilayer structures. Most transition metals have incomplete filled d-shell orbitals. This means that there are vacant orbitals in the valence band that allows for electronic transitions once the material is irradiated by electromagnetic waves (Bewick *et al.,* 2009; Lee & Wu, 2017; Han *et al.,* 2021).

Zinc and its derivative such as zinc sulphide (ZnS) are widely used in optical and electronics devices for infrared windows and flat panel displays because of its wide band gap (3.7 eV), low optical absorption in the visible and infrared spectral regions (Daranfed *et al.,* 2009). In addition to a wide band gap, this compound also has a high refractive index of n = 2.35, high transmittance (> 90% in the visible wavelength range) (Cheng, 2003). On the other hand, silver (Ag) is a remarkably good optical material with low absorption in the visible region and high reflectance in the infrared region and frequency dependent refractive index (Sinha *et al.,* 2006; Chou *et al.,* 2020). The additional technical quality of silver at nanoscale is that of high chemical and optical activity with the capacity to permeate or fuse with dielectric materials to form hybrid semiconductor layers (Morton *et al.,* 2011; Priyadharsini *et al.*, 2016).

When depositing metal films, the vapour flux coming from evaporating material may reach the substrate normally or at some other angle. Research on film deposition processes reveals that, at normal incident, the vapour flux upon deposition tends to form a relatively homogeneous film (Lintymer *et al.,* 2003; Pedrosa *et al.,* 2017). However, when the angle of deposition increases, the film's homogeneity tends to reduce rendering the film to have a relatively rough surface but also change in its

internal microstructure (Taschuk *et al.,* 2010). During oblique deposition, the initial particles are formed on substrate but this may hinder the direct adhesion of preceding atoms. Along the direction of initially deposited atoms, columns are formed that shadow the incoming vapour atoms from reaching directly to the substrate surface (Charles *et al.,* 2015). This forms atomic islands with restricted adatom mobility and surface diffusion of deposited particles. This phenomenon leads to formation of a porous microstructure that affects the film density, reflectance, transmittance, absorbance and electrical conductivity of the thin film materials (Sobahan *et al.,* 2009; He *et al.,* 2014).

When an electromagnetic radiation is incident on the surface of nanostructures such as Ag and ZnS, electrical oscillations of conduction electrons takes place on the surface of the metal. These electrical oscillations are called localized surface plasmons (Chalana *et al.,* 2015). The excitation of surface plasmons by an external electrical field results in charge polarization on the metal surface. At resonance point (point at which frequency of applied field is equal to frequency of waves from electrical excitation), surface plasmon resonance occurs which leads to strong absorption or scattering of incident light. Surface plasmon absorption bands of Ag are in the visible and near-infrared spectral regions. This is very useful for technological applications. When Zinc sulphide nanoparticles are subjected to the external electromagnetic field, coherent oscillations (surface Plasmon resonance) of the conduction electrons also occurs (Venugopal & Mitra, 2013). Surface plasmon effects are however, governed by several factors which include frequency of incident radiation, film thickness and formation of atomic islands on the surface of the dielectric substrate. Notably, film thickness and deposition angle present a profound effect on spectral properties of thin film nanostructures.

Although many deposition studies have been done on zinc sulphide and silver thin films, less attention has been placed on effect of film thickness (less than 20 nm) and angle of deposition of ZnS/Ag multilayers. Thus, this paper presents the transmittance properties of thermally evaporated coatings of ZnS/Ag as a function of film thickness and deposition angle, in addressing the challenges of indoor heating.

Materials and Methods

The microscope glass slides of dimensions 76 × 25×1mm^3 were thoroughly cleaned with a soap solution of sodium silicate, 2-butoxyethtanol in an ultrasonic cleaner for 20 minutes and rinsed by ethanol vapor followed by distilled water in a clean environment before placing them in high vacuum system for deposition.

The deposition of ZnS/Ag thin films was performed in two steps while varying the film thickness and the deposition angle. Silver metal wire (99.99% purity) was heated on a refractory tantalum boat under vacuum at a pressure of 2.5×10^{-5} mBars and deposited on glass slide substrates in the diffusion pump microprocessor vacuum coater (Edwards AUTO 306). The heating current was slowly raised to 38 A and an evaporation rate of 1 nms^{-1} was used to deposit the evaporated silver metal. Utmost care was taken to ensure that current was maintained at 36 A for silver metal in all samples. Silver metal has a low melting point and high current would evaporate all the silver on the refractory boat. Glass slides were fixed on a rotary holder using cello tape of vacuum laboratory grade. The glass slides were placed 11 cm away from the refractory boat vertically above it.

The substrate holder together with the glass slide was rotated at an angle θ about the horizontal so that the vapour is incident at an angle θ, to the substrate normal (the angle between the normal to the substrate and direction of incidence of the evaporated atoms). The setup is shown in Figure 1. Three sets of samples of silver films of thickness 4 nm were deposited at different angles of $\theta = 0^o$, 30^o and 60^o onto glass substrate. This was repeated for each of thickness of 7, 10 and 15 nm.

The thickness of silver films was measured by a thickness monitor connected to a quartz crystal monitoring system placed inside the diffusion vacuum chamber. The quartz crystal was calibrated for the density and acoustic impedance using standard data from vacuum systems. The thickness was also calibrated so that substrate

shutter and the crystal monitor could automatically close once a particular thickness was reached.

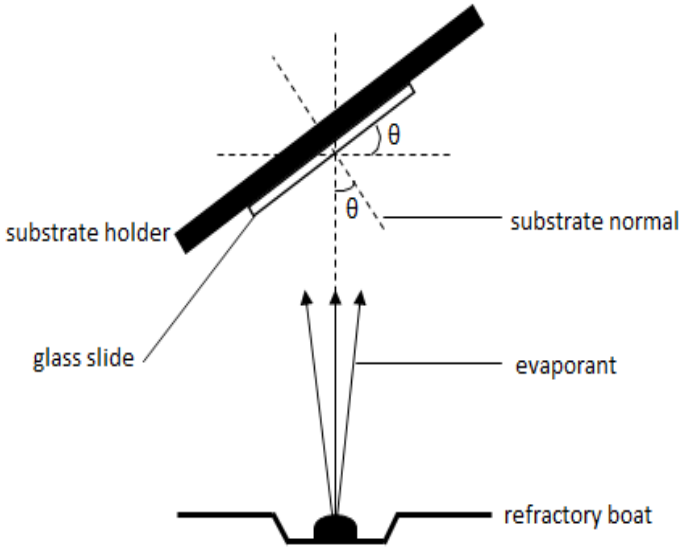

Figure 1. Setup for Vacuum vapor deposition

The pieces of ZnS (99.99% purity) were heated in a molybdenum boat with source cover to reduce the spreading of the ZnS vapour. The heating current was increased slowly to 56 A. It was very necessary to carefully control the heating current because at larger currents greater than 56 A, a lot of vapour from ZnS could fill the chamber. This would compromise the accuracy of the crystal monitor inside the vacuum chamber. The thickness of ZnS films was measured by a thickness monitor connected to a quartz crystal monitoring system placed inside the diffusion vacuum chamber. The quartz crystal was recalibrated for the density and acoustic impedance of ZnS using standard data from vacuum systems. The thickness was also calibrated so that substrate shutter and the crystal monitor could automatically close once a particular thickness was reached. The ZnS was heated and deposited to film thickness of 4 nm at vapour incidence angle $\theta = 0^o$, 30^o and 60^o to the glass slides previously coated with silver to form the ZnS/Ag/glass multilayer system shown in Figure 2. This procedure was repeated for thicknesses 7, 10 and 15 nm.

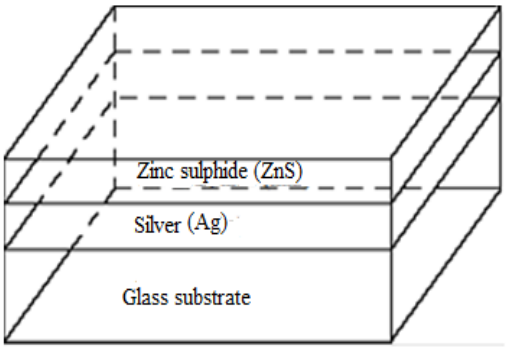

Figure 2. Composite of the ZnS/Ag/glass system

The optical transmittance of the samples was studied by the UV/Vis/NIR spectrometer (Perkin Elmer Lambda 19) with UV-WinLab software. This is a double beam instrument covering the ultraviolet, visible and near infrared spectral regions. Baseline measurement using a clean piece of substrate was done. The transmittance of obliquely evaporated coatings was measured at normal incidence in the wavelength range of 250-2500 nm (Drakopoulos *et al.*, 2005). The data obtained was analysed by OriginLab software.

Results

Transmittance of ZnS(θ^o)/Ag(0^o) for different thickness and deposition angle

The spectrophotometric data was obtained in the wavelength range of 250 - 2500 nm. The results have been presented from three perspectives with three variables. The variables were film thickness of ZnS/Ag, deposition angle of zinc sulphide and silver. Inset, the first figure in brackets, (θ) after ZnS represents the angle of deposition (AOD) of ZnS nanostructures, while the figure in the second brackets, (θ) after Ag represents the angle of deposition (AOD) of Ag nanostructures. Also both in the text and in the figure legends, the figure in nanometres (nm) in front of ZnS/Ag refers to the film thickness of both ZnS and Ag.

The transmittance values for different film thicknesses i.e. 4, 7, 10 and 15 nm for ZnS/Ag nanostructures are shown in Figure 3a. The transmittance was observed to increase with decrease in film thickness of normally deposited ZnS/Ag nanostructures. The transmittance of the ZnS(0^o)/Ag(0^o) nanostructures decreased from the visible short wavelength towards the near infrared wavelengths. The transmittance peaks in the visible region for (4 nm)ZnS(0^o)/Ag(0^o), (7 nm)ZnS(0^o)/Ag(0^o), (10 nm)ZnS(0^o)/Ag(0^o) and (15 nm)ZnS(0^o)/Ag(0^o) were 61.7%, 66.3%, 54.9%, and 18.0% respectively. There was a very sharp rise in transmittance at about 350 nm wavelengths for all samples. The transmittance peaks however, decreased towards the longer wavelengths. The (4 nm)ZnS(0^o)/Ag(0^o) nanostructured multilayer films had exceptionally high transmittance values with a peak at 61.7% in the visible and 21.9% in the infrared region at λ = 1800 nm.

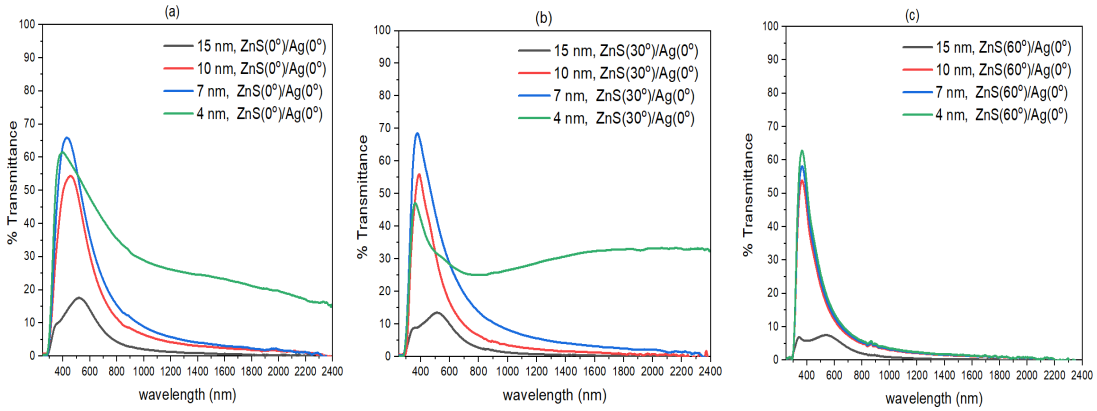

Figure 3. Variation of Transmittance with film thickness and deposition angle of ZnS when the deposition angle of Ag nanostructures was fixed at 0^o

Transmittance of ZnS(θ°)/Ag(30°) for different thickness and deposition angles *In this section, zinc* sulphide was deposited from normal to oblique angle on obliquely evaporated silver films. Here the Ag nanostructures were deposited at an oblique angle of 30° to the substrate normal to form nanostructures of different thicknesses. When the deposition angle of the multilayers was increased from ZnS(0°)/Ag(0°), to ZnS(0°)/Ag(30°) (Figure 4a) for different thicknesses, it was observed that the optical transmittance increased with decrease in film thickness for different nanostructures. The transmittance values at λ = 1800nm for (4 nm)ZnS(0°)/Ag(30°), (7 nm)ZnS(0°)/Ag(30°), (10 nm)ZnS(0°)/Ag(30°), (15 nm)ZnS(0°)/Ag(30°) were 28.0%, 21.7%, 4.5% and 0.7% respectively.

When the deposition angle of ZnS was increased to 30°, i.e from ZnS(0°)/Ag(0°) to ZnS(30°)/Ag(30°) Figure 4b, there was a slight decrease in optical transmittance in the visible region. The optical transmittance increased with decrease in film thickness. The transmission peaks in the visible spectrum increased towards the long wavelength. The transmittance values at λ = 1800 nm for (4 nm)ZnS(30°)/Ag(30°), (7 nm)ZnS(30°)/Ag(30°), (10 nm)ZnS(30°)/Ag(30°) and (15 nm)ZnS(30°)/Ag(30°) were 17.9%, 21.1%, 4.6% and 0.5% respectively.

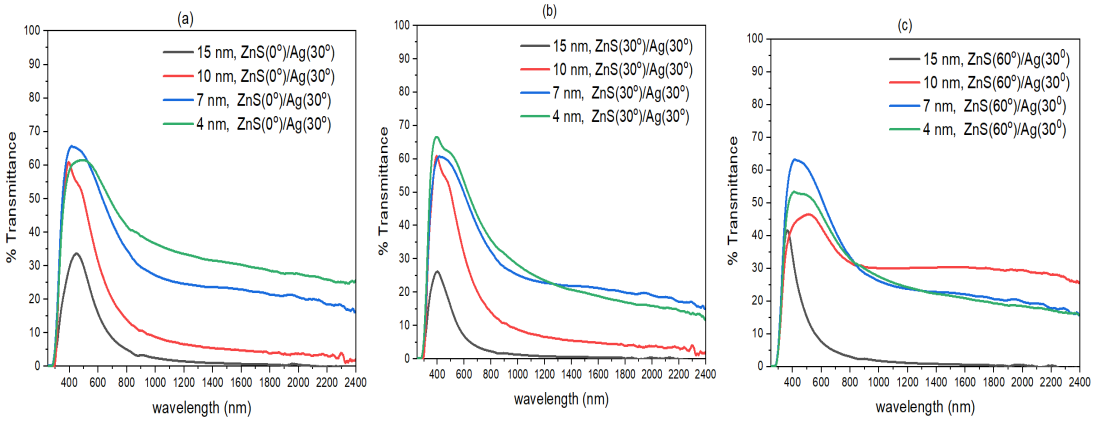

Figure 4. Variation of Transmittance with thickness and deposition angle of ZnS when the deposition angle of Ag was held at 30°

When the deposition angle of ZnS was increased to 60° i.e (4 nm)ZnS(60°)/Ag(30°), (7 nm)ZnS(60°)/Ag(30°), (10 nm)ZnS(60°)/Ag(30°) and (15 nm)ZnS(60°)/Ag(30°) (Figure 4c), the transmittance values for different film thicknesses decreased in the visible while the transmittance in the infrared region increased. The transmittance peaks in the visible wavelength for (4 nm)ZnS(30°)/Ag(30°), (7 nm)ZnS(30°)/Ag(30°), (10 nm)ZnS(30°)/Ag(30°) and (15 nm)ZnS(30°)/Ag(30°) were 53.8%, 63.6%, 47.2% and 42.4% respectively. While the transmittance in the infrared at λ = 1800 nm for (4 nm)ZnS(30°)/Ag(30°), (7 nm)ZnS(30°)/Ag(30°), (10 nm)ZnS(30°)/Ag(30°) and (15 nm)ZnS(30°)/Ag(30°) were 20.1%, 21.7%, 30.6% and 0.1% respectively.

Transmittance of ZnS(θ°)/Ag (60°) for different thickness and deposition angle

Consider a multilayer nanostructured film formed by normal deposition of ZnS on obliquely deposited silver at 60°, i.e ZnS(0°)/Ag(60°) Figure 5a. The transmittance response as a function film thickness, generated decreased transmittance values in the visible region with a broad transmission band. The transmittance values in the visible wavelength were 54.8%, 62.1%, and 61.8% for (4 nm)ZnS(0°)/Ag(60°), (7 nm)ZnS(0°)/Ag(60°) and (10 nm)ZnS(0°)/Ag(60°) respectively. In the infrared region, the transmittance values were 47.4%, 22.0% and 3.2% for (4 nm)ZnS(0°)/Ag(60°), (7 nm)ZnS(0°)/Ag(60°) and (10 nm)ZnS(0°)/Ag(60°) respectively. The transmittance of the specimens increased with decrease in film thickness with the increase in deposition angle of Ag. Though the transmittance values for (4 nm)ZnS(0°)/Ag(60°) and (7 nm)ZnS(0°)/Ag(60°) and (10 nm)ZnS(0°)/Ag(60°) in the visible region was above 55%, the transmittance of these samples in the entire infrared region is relatively high.

When the deposition angle of ZnS was increased to 30° i.e ZnS(30°)/Ag(60°) (Figure 5b), the transmission peaks in the visible spectrum decreased to 60.4%, 45% and 6.4% for specimen (4 nm)ZnS(30°)/Ag(60°), (7 nm)ZnS(30°)/Ag(60°) and (10 nm)ZnS(30°)/Ag(60°) respectively. While in the infrared wavelength, the transmittance values at λ = 1800 nm were 60.4%, 45.8% and 6.4% for (4 nm)ZnS(30°)/Ag(60°), (7 nm)ZnS(30°)/Ag(60°) and (10 nm)ZnS(30°)/Ag(60°) respectively. The transmittance of (4 nm)ZnS(30°)/Ag(60°) and (7 nm)ZnS(30°)/Ag(60°) increased towards the long wavelength in the infrared region. Hence, the transmittance in the infrared region exceeded that in the visible band of the electromagnetic spectrum.

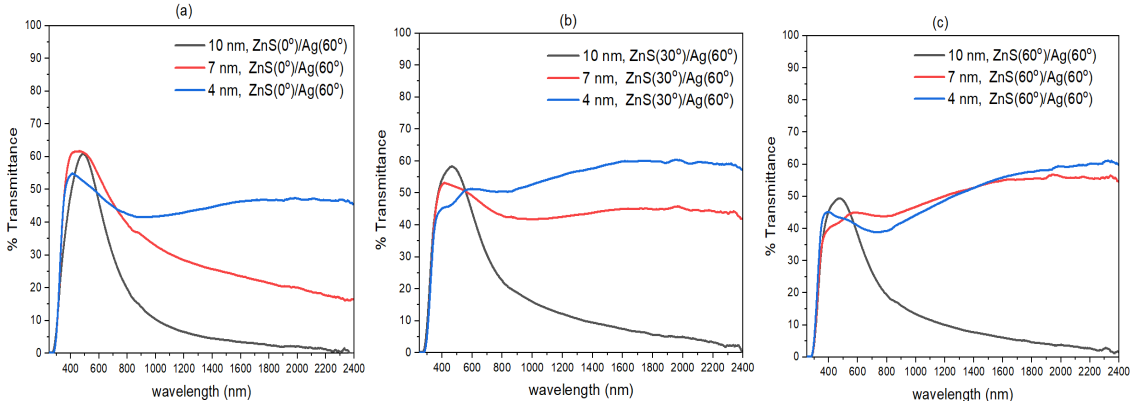

Figure 5. Variation of transmittance with thickness and deposition angle of ZnS when the deposition angle of Ag was fixed at 60°

Further increase in the deposition angle of ZnS to 60° i.e ZnS(60°)/Ag(60°) Figure 5c, the optical transmittance peaks in the visible wavelength were nearly equal i.e they were standing on shoulder by shoulder for (4 nm)ZnS(60°)/Ag(60°) and (7 nm)ZnS(60°)/Ag(60°) nanostructures. The transmittance in the infrared region at around λ = 1700 nm decreased with thickness of ZnS/Ag nanostructures. Therefore, the optical transmittance in the visible region had peaks at 45.7%, 45.4% and 49.6% for (4 nm)ZnS(60°)/Ag(60°) and (7 nm)ZnS(60°)/Ag(60°) and (10 nm)ZnS(60°)/Ag(60°) nanostructures respectively. In the infrared wavelengths, the transmittance values for (4 nm)ZnS(60°)/Ag(60°),

(7 nm)ZnS(60°)/Ag(60°) and (10 nm)ZnS(60°)/Ag(60°) nanostructures at λ = 1800 were 58.2%, 56.2% and 5.0% respectively. The transmittance of the specimen in the visible region was less than the transmittance in the infrared region. The transmittance values in the infrared region exceeded the transmittance in the visible region by ≈ 15%.

Transmittance of (10 nm)ZnS/Ag with angular deposition of silver

This section examines the effect of deposition angle of silver nanostructures on the optical transmittance of (10 nm)ZnS/Ag nanostructures. In Figure 6a, silver metal nanostructures were separately deposited at 0°, 30° and 60° to substrate normal of the glass slides. This was followed by the deposition of zinc sulphide films normally (i.e. at 0°) to the substrate normal on each of the slides. The transmittance peaks for ZnS(0°)/Ag(30°) and ZnS(0°)/Ag(60°) (i.e. T = 61.3%) were higher than for ZnS(0°)/Ag(0°) (T = 53.9%) in the visible spectrum.

When the deposition angle of ZnS was increased to 30° Figure 6b, the transmittance in the visible region was slightly decreased. The transmittance values in the visible region had peaks at 55.8%, 48.6% and 58.4% for ZnS(30°)/Ag(0°), ZnS(30°)/Ag(60°) and ZnS(30°)/Ag(60°) respectively. Whereas in the infrared region, the transmittance increased slightly with the deposition angle of Ag, there was a general increase in transmittance in the infrared region due to 30° oblique deposition angle of ZnS. The transmittance values in the infrared region were slightly higher and dispersed than those obtained in infrared region as shown in Figure 6a.

When the deposition angle of ZnS was further raised to 60° (Figure 6c), the transmittance in the visible region was further reduced. The transmission peaks in the visible spectrum were 54.9%, 47.3% and 50.1% for specimen ZnS(60°)/Ag(0°), ZnS(60°)/Ag(60°) and ZnS(60°)/Ag(60°) respectively. The transmittance values however, further increased in the infrared region due to high deposition angle of ZnS.

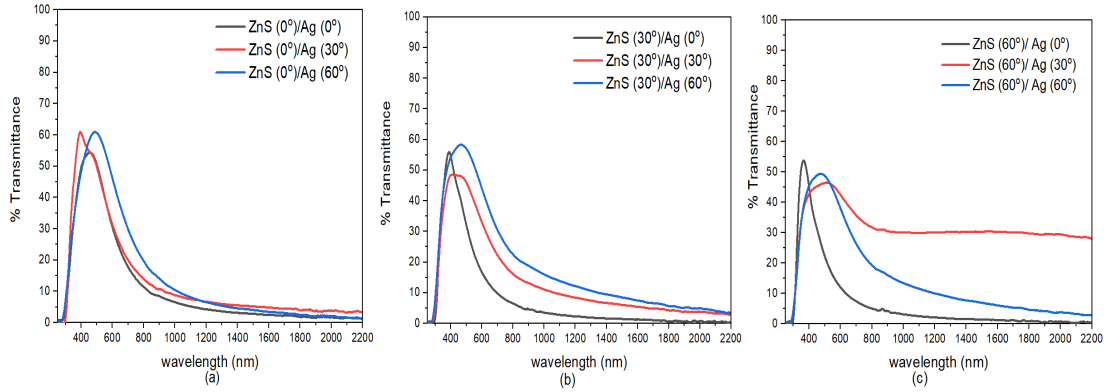

Figure 6. Effect of deposition angle of Ag on transmittance of (10 nm) ZnS/Ag films at constant angle of deposition of ZnS

Transmittance of (7 nm)ZnS/Ag with angular deposition of silver

The transmittance of (7 nm)ZnS(0°)/Ag(0°) had generally high transmittance values of <61% in the visible spectrum, Figure 7a. The transmittance of the specimens decreased towards the infrared region. Increase in deposition angle of Ag increased the transmittance in the infrared wavelengths. The transmittance in the infrared at λ = 1800 nm for ZnS(0°)/Ag(0°), ZnS(0°)/Ag(30°) and ZnS(0°)/Ag(60°) were 2.8%, 21.7% and 22.1% respectively.

When the deposition angle of ZnS was increased from 0° to 30°, i.e. ZnS(30°)/Ag (Figure 7b), the transmittance of samples; ZnS(0°)/Ag(30°) and Zn(0°)/Ag(60°) decreased in the visible spectrum with the transmittance peaks decreasing towards the infrared region. The peak values for

ZnS(0°)/Ag(0°), ZnS(0°)/Ag(30°) and ZnS(0°)/Ag(60°) in the visible region were 68.2%, 61.3% and 53.7% respectively. The transmittance values of ZnS(0°)/Ag(0°), ZnS(0°)/Ag(30°) and ZnS(0°)/Ag(60°) in the infrared at λ = 1800 nm were 2.6%, 21.0% and 45.4% respectively. Comparatively, there was a slight decrease in transmittance in the visible region and an increase in transmittance in the infrared region. As the deposition angle of Ag was increased to (60°) the transmittance increased to more than 45% in the infrared region.

Three slides coated with Ag at deposition angle of 0°, 30° and 60° were then coated with ZnS at deposition angle of 60°. The spectrophotometric data is as shown in Figure 7c. The transmittance values for ZnS(60°)/Ag(0°), ZnS(60°)/Ag(30°) and ZnS(60°)/Ag(60°) in the visible spectrum were 51.2%, 53.7% and 45.9% respectively. The optical transmittance of ZnS(60°)/Ag(0°) and ZnS(60°)/Ag(30°) samples in the infrared region was lower than the transmittance in the visible region. The transmittance values in the infrared were 35.7%, 18.6% and 58.0% for ZnS(60°)/Ag(0°), ZnS(60°)/Ag(30°) and ZnS(60°)/Ag(60°) respectively. Nevertheless, the transmittance of ZnS(60°)/Ag(60°) in the infrared region was slightly higher than the transmittance in the visible region.

Transmittance of (4 nm)ZnS/Ag with angular deposition of silver

The (4 nm)ZnS(0°)/Ag(0°) samples had above average values of transmittance in the visible range with peak values of 62.1%, 61.7% and 55.2% for (4 nm)ZnS(0°)/Ag(0°) and (4 nm)ZnS(0°)/Ag(30°) and (4 nm)ZnS(0°)/Ag(60°) respectively, Figure 8a. The transmittance values in the infrared region were below average values in the infrared spectral region. Thus, the transmittance values in the infrared wavelengths were 21.5%, 25.5%, and 47.3% for specimen (4 nm)ZnS(0°)/Ag(0°) and (4 nm)ZnS(0°)/Ag(30°) and (4 nm)ZnS(0°)/Ag(60°) respectively. The transmittance values of (4 nm)ZnS(0°)/Ag(0°) and (4 nm)ZnS(0°)/Ag(30°) in the infrared region were measurably low to allow for the strong transmission of short wavelength infrared radiation. However, when the deposition angle of Ag was raised to (4 nm)ZnS(0°)/Ag(60°), the transmittance in the infrared region increased.

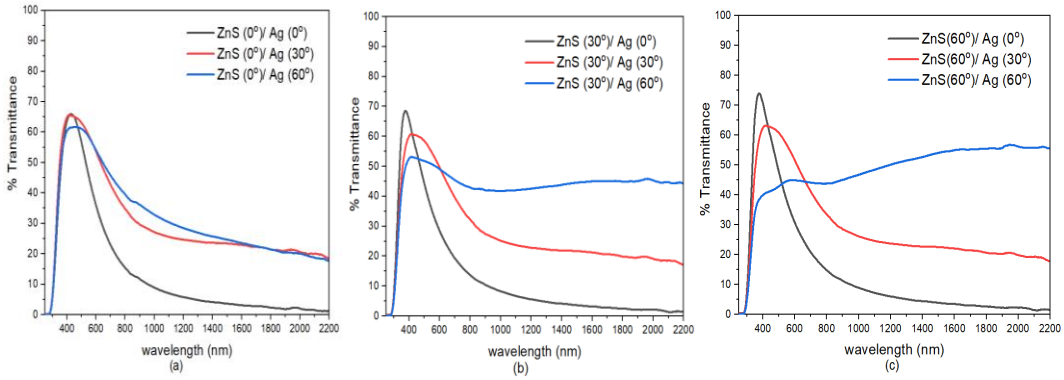

Figure 7. Effect of deposition angle of Ag on transmittance of (7 nm) ZnS/Ag films at constant angle of deposition of ZnS

When the deposition angle of ZnS was increased to 30° Figure 8b, the transmittance of (4 nm)ZnS(30°)/Ag(0°) and (4 nm)ZnS(30°)/Ag(30°) increased with increase in deposition angle of Ag films in the visible region. The transmittance values for (4 nm)ZnS(0°)/Ag(0°) and (4 nm)ZnS(0°)/Ag(30°) and (4 nm)ZnS(0°)/Ag(60°) in the visible were 47.5%, 67% and 51.5% respectively. Nevertheless, the decrease in transmittance in the visible region could be noticed in samples ZnS(30°)/Ag(0°) and ZnS(30°)/Ag(30°) but with still lower transmittance values in the infrared region. Though the deposition angle of Ag was high, the reflectance could have been amplified by the deposition angle of ZnS.

When the deposition angle of ZnS was increased to 60° Figure 8c, the transmittance values of ZnS/Ag films in the visible region ware slightly reduced. The transmittance peak values were 51.1%, 53.5%, and 45.1% for (4

nm)ZnS(0°)/Ag(0°) and (4 nm)ZnS(0°)/Ag(30°) and (4 nm)ZnS(0°)/Ag(60°) respectively. Thus, increasing the deposition angle of ZnS decreased transmittance in the visible wavelength. At high deposition angle of ZnS, the transmittance in the infrared range increased in comparison to transmittance values in Figure 8b and 8a.

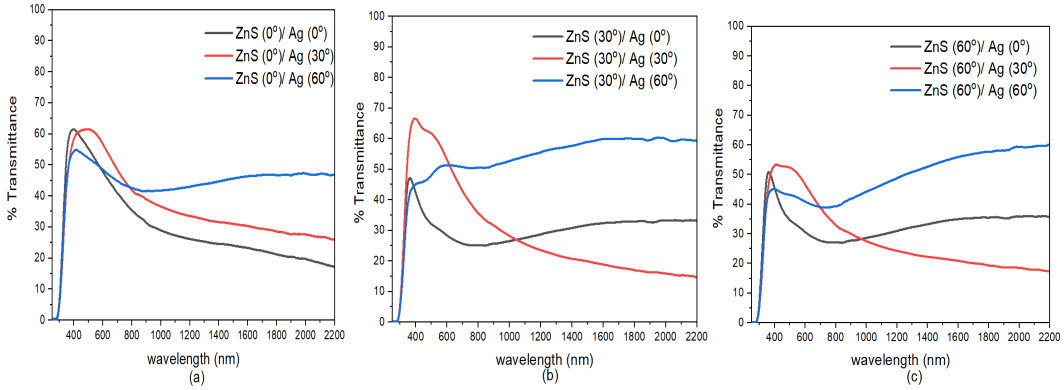

Figure 8. Effect of deposition angle of Ag on transmittance of (4 nm)ZnS/Ag films at constant angle of deposition of ZnS

Discussion

Effect of thickness and deposition angle on transmittance of ZnS/Ag(0°)

The results presented in Figure 3 show that the (4 nm)ZnS(0°)/Ag(0°) nanostructures were transparent to both visible light and infrared light. The high transmittance values in the infrared do not permit this specimen for applications involving thermal infrared reflectors. This was due to low absorption of light by Ag nanoparticles (Kavei & Nikbin, 2015). The transmittance of the samples in the visible region exhibited strong absorption bands due to partially filled d-orbitals of Ag and Zn atoms (Rahmani *et al.,* 2009). In separate studies by Hossain *et al.,* (2014) and Jolly *et al.,* (2012), the broad transmittance bands observed in the visible region could be due to surface plasmon resonance of the Ag nanoparticles present in the ZnS dielectric nanostructures (Pan *et al.,* 2020).

When the deposition angle of ZnS was increased to 30° Figure 3b, the transmission bands in the visible spectrum became narrow with reduced values of optical transmittance. The increase in deposition angle of ZnS increased transmittance in the infrared wavelengths. Further increase in the deposition angle of ZnS to 60° Figure 3c, the transmittance peaks in the visible wavelength showed very little change. The low transmittance values of the samples at the long wavelength were as result of optical loss due to absorption and scattering of infrared photons (Ye *et al.,* 2019).

Effect of thickness and deposition angle on transmittance of ZnS/Ag(30°)

When the deposition angle of silver was increased to 30° (Figure 4a), the optical transmittance increased with decrease in film thickness. The increase in optical transmittance of the ZnS/Ag nanostructures was due to the decrease in optical scattering as a result of the decrease in density of the grain boundaries. However, the optical transmittance was enhanced both in the visible and the infrared wavelengths by the oblique deposition of silver. Thus, the deposition angle of silver had a profound effect on the optical transmittance of electromagnetic radiation (Yildiz *et al.,* 2015).

When the deposition angle of ZnS was increased to 60°, Figure 4c, the transmittance values decreased in the visible while the transmittance in the infrared region increased. This increase was due to a combined effect of deposition angle of ZnS and Ag and the high refractive index of ZnS (Ahmad *et al.,* 2017). The broad transmission bands between 380 to 800 nm were due to inter-band electronic transitions of the filled 3d-electron orbitals of the Zn and Ag atoms and the effect of photon absorption of the glass substrate (Kreibig & Vollmer, 2013; Rahchamani *et al.,* 2015; Yildiz *et al.,* 2015). The low value of optical transmittance of (15 nm)ZnS/Ag thin films was

because of the high absorption by the (15nm)Ag mid-layer and the glass substrate (Ye *et al.,* 2019). According to (Sivaramakrishnan & Alford, 2009) and (He *et al.,* 2014), the increase in transmittance in the visible region could be explained by the formation of discontinuous Ag islands on glass substrate.

Effect of thickness and deposition angle on transmittance of ZnS/Ag (60^o)

The transmittance of ZnS(0)/Ag(60) nanostructures Figure 5a, increased with decrease in film thickness but increased with increase in deposition angle of Ag. Though the transmittance values in the visible region were above 55%, the transmittance of these samples in the entire infrared region was relatively high. The high optical transmittance of the specimens was due to the high optical absorption by the ZnS/Ag multilayer nanostructures (Pandey *et al.,* 2014). According to Macleod (2010), during the normal deposition process of ZnS, the incident vapour flux creates densely packed film structures which are relatively homogeneous.

When the deposition angle of ZnS was increased to 30^o Figure 5b, the transmittance of (4 nm)ZnS(30^o)/Ag(60^o) and (7 nm)ZnS(30^o)/Ag(60^o) in the infrared region increased with increase in deposition angle of ZnS. This was brought about by the combined effect of the oblique deposition of both ZnS and Ag nanostructures. Hence these samples were more transparent to infrared light than the visible light. This implies that (7 nm)ZnS/Ag sample worked better as a heat mirror at low deposition angle of ZnS and high deposition angle of Ag.

The transmittance of (10 nm)ZnS(30^o)/Ag(60^o) in the visible spectrum was higher than the transmittance in the infrared wavelengths. This specimen was a good transmitter in the visible wavelength but poor transmitter in the infrared wavelength. Further increase in the deposition angle of ZnS to 60^o Figure 5c, the optical transmittance peaks in the visible wavelength were nearly equal for (4 nm)ZnS(60^o)/Ag(60^o) and (7 nm)ZnS(60^o)/Ag(60^o) nanostructures. In a study by Chalana *et al.,* (2015) on surface plasmon resonance in nanostructured films, the decrease in transmittance was attributed partly to enhanced absorption of electromagnetic radiation by silver nanoparticles and atomic shadowing due to limited adatom diffusion of the ZnS nanoparticles. Hence, for this particular specimen the deposition of ZnS should be restricted to normal deposition.

Angular deposition of Ag on transmittance of (10 nm)ZnS/Ag

The transmittance peaks for ZnS(0^o)/Ag(30^o) and ZnS(0^o)/Ag(60^o) Figure 6a, were above average in the visible spectrum. This showed that the oblique angle deposition of Ag enhanced optical transmission in the visible region. The transmittance then decreased from the visible towards the infrared spectral wavelengths. Nonetheless, the transmittance in the infrared region increased with the deposition angle of Ag nanostructures. When the deposition angle of ZnS was increased to 30^o Figure 6b, the transmittance in the visible region was slightly decreased. Whereas in the infrared region the transmittance increased with the deposition angle of Ag. There was a general increase in transmittance in the infrared region due to 30^o oblique deposition angle of ZnS.

When the deposition angle of ZnS was further raised to 60^o Figure 6c, the transmittance in the visible region was further reduced while the transmittance values were further increased in the infrared region (Taschuk *et al.,* 2010).

The physical significance of this behavior was that oblique angle deposition had a negative contribution to transmittance in visible region and a positive contribution in the infrared region.

Angular deposition of Ag on transmittance of (7 nm)ZnS/Ag

The transmittance of (7 nm)ZnS(0)/Ag(0) decreased towards the infrared region Figure 7a. However, angular deposition effects were weekly pronounced in the visible region. When the deposition angle of ZnS was increased from 0^o to 30^o Figure 7b, the transmittance of samples decreased in the visible spectrum with the transmittance peaks decreasing towards the infrared region. When the deposition angle of ZnS was increased to 60^o Figure 7c, the transmittance in the visible region slightly increased while the optical transmittance of the samples in the infrared region decreased.

Nevertheless, the transmittance of ZnS(60^o)/Ag(60^o) in the infrared region was slightly higher than the transmittance of ZnS(30^o)/Ag(60^o), Figure 7b. This could be attributed to increase in homogeneities (discontinuities in the ZnS/Ag nanostructured layers) due to atomic shadowing during the formation of the ZnS and Ag films on the glass substrate. This increased optical absorption and hence transmittance to about 55% in the infrared region (Macleod, 2010; Vrakatseli *et al.,* 2018).

Angular deposition of Ag on transmittance of (4 nm)ZnS/Ag

The (4 nm)ZnS(0^o)/Ag(0^o) samples had above average values of transmittance in the visible range, Figure 8a and below average values in the infrared spectral region. However, when the deposition angle of Ag was raised to 60^o, the transmittance in the infrared region increased. When the deposition angle of ZnS was increased to 30^o Figure 8b, the transmittance of (4 nm)ZnS(30^o)/Ag(0^o) and (4 nm)ZnS(30^o)/Ag(30^o) in the visible region increased with increase in deposition angle of Ag films. Nevertheless, the decrease in transmittance in the visible region could be noticed in samples ZnS(30^o)/Ag(0^o) and ZnS(30^o)/Ag(30^o) but with still lower transmittance values in the infrared region. The decrease in transmittance was due to the increase in deposition angle of ZnS. The optical transmittance of (4 nm)ZnS(0^o)/Ag(60^o) in the infrared was higher than that in the visible region. Though the deposition angle of Ag was high, the transmittance could have been amplified by the deposition angle of ZnS. The high transmittance was attributed to the small grain size of the ZnS and Ag nano-particles and the effect of deposition angle of very thin films (Sobahan *et al.,* 2009).

When the deposition angle of ZnS was increased to 60^o Figure 8c, the transmittance values of ZnS/Ag nanostructures in the visible region ware slightly reduced. Thus, increasing the deposition angle of ZnS decreased transmittance in the visible wavelengths. This trend according to Al-Ofi *et al.,* (2012) was due to increase in both reflection and absorption in the nanostructures in the visible region (Abd El-Raheem *et al.,* 2016; Abd El-Raheem, *et al.,* 2017).

Conclusion

The nanostructures formed by normally and obliquely evaporating ZnS/Ag nanostructures on glass substrate showed that; the optical transmittance in the visible region was enhanced by the deposition of silver nanoparticles at higher deposition angles. However, the deposition of Ag nanoparticles at high deposition angles suppressed the optical transmittance in the infrared region. Therefore, it was recommended that for high transmission in the visible and good thermal infrared control, silver nanoparticles should be deposited at higher deposition angles. The deposition of ZnS at high deposition angle decreased transmittance in the visible wavelength but increased transmittance in the infrared wavelengths. Hence, to increase transmittance in the visible region and minimise infrared transmittance, Zinc sulphide should be coated on silver at low deposition angles.

The transmittance values for (15 nm)ZnS/Ag at different deposition angles was less than 20.0% in the visible spectrum and less than 8.0% in the infrared region. The (15nm) ZnS/Ag film progressively became opaque with increase in deposition angle of ZnS in the wavelength range $\lambda > 1000$ nm. Therefore, these samples were regarded to be opaque to both visible light and infrared radiation. These samples could not be adapted for use in transparent nanostructures.

The transmittance for (10 nm)ZnS/Ag and (7 nm)ZnS/Ag in the visible wavelengths were above average (< 50%), and (< 20%) the in the infrared region. Therefore, these structures can be considered as a transparent to the visible light with limitation to transmittance of infrared radiation. When the deposition angle of zinc sulphide was increased to 60^o the ultrathin (7 nm)ZnS/Ag nanostructures were more transparent to infrared electromagnetic radiation but less transparent to visible light. The (4 nm)ZnS/Ag nanostructure at different deposition angles had average transmittance values in the visible spectrum. The transmittance values in the infrared region were generally higher than those in the visible. Therefore, this structure was transparent to both visible light and thermal infrared radiation.

At longer wavelengths, transmittance decreased rapidly with increase in film thickness. This implies that the less energetic infrared light could not pass through the nanostructures. When the deposition angle of Ag was kept constant while the deposition angle of ZnS was increased in the ZnS/Ag multilayer structures, the transmittance in the visible region decreased while the transmittance in the infrared wavelength increased. However, the (4 nm)ZnS/Ag at different deposition angles had above average transmittance values in the near infrared spectral wavelength. These structures exhibited properties of poor heat mirrors in the infrared wavelengths.

Acknowledgments

The Authors would like to acknowledge the financial and material support from SIDA (The Swedish International Cooperation Agency) through ISP (the International Science Programme, Uppsala University) and Uganda Independent Scholarships Trust Fund Board, Ministry of Education and Sports.

References

Abd El-Raheem, M., Atta, A., Amry, A., Al-Baradi, A. M., Alomairy, S. E., Alkhammash, H., and Amin, S. (2017). Study on transparent oxides thin films prepared using sputtering method. *Journal of Computational and Theoretical Nanoscience,* 14(5):2501–2507.

Abd El-Raheem, M., Diab, A., Alhuthali, A., and Al-Baradi, A. M. (2016). Effect of gas pressure and film thickness on the optical constants of transparent conducting oxide based on zinc oxide. *Journal of Optical Technology*, 83(1):30–35.

Ahmad, S., Al-Kuhaili, M., Durrani, S., Faiz, M., and Ul- Hamid, A. (2017). Bi-layered energy efficient coatings as transparent heat mirrors based on vanadium oxide thin films. *Solar Energy Materials and Solar Cells*, 169:258–263.

Al-Ofi, H., Abd El-Raheem, M., Al-Baradi, A. M., and Atta, A. (2012). Structural and optical properties of Al_2ZnO_4 thin films deposited by dc sputtering technique. *Journal of non-oxide glasses*, 3(3):39–54.

Bewick, S., Edge, J., Forsythe, T., and Parsons, R. (2009). *CK12 Chemistry*. CK-12 Foundation.

Bwayo, E. and Obwoya, S. (2014). Coefficient of thermal diffusivity of insulation brick developed from sawdust and clays. *Journal of ceramics*, 2014.

Charles, C., Martin, N., and Devel, M. (2015). Optical properties of nanostructured WO_3 thin films by glancing angle deposition: Comparison between experiment and simulation. *Surface and Coatings Technology*, 276:136–140.

Chalana, S., Ganesan, V., and Mahadevan Pillai, V. (2015). Surface plasmon resonance in nanostructured Ag incorporated ZnS films. *Advances*, 5(10):107207.

Cheng, J. (2003). DB Fan. H. Wang. Bw Liu. Yc Zhang. H. Yan. *Semicond. J. Sci. Technol*, 18:676.

Chou, C.-H., Lin, Y. T., Shinde, S., Huang, C.-E., Wu, T.-C., Lin, K.-M., and Hsiao, W. T. (2020). The development of a monitoring system for analyzing factors affecting film thickness in a sputtering process. *Modern Physics Letters* B, 34(07n09):2040021.

Dalapati, G. K., Kushwaha, A. K., Sharma, M., Suresh, V., Shannigrahi, S., Zhuk, S., & Masudy-Panah, S. (2018). Transparent heat regulating (THR) materials and coatings for energy saving window applications: Impact of materials design, micro-structural, and interface quality on the THR performance. *Progress in materials science*, *95*, 42-131.

Daranfed, W., Aida, M., Hafdallah, A., and Lekiket, H. (2009). Substrate temperature influence on ZnS thin films prepared by

ultrasonic spray. *Thin Solid Films*, 518(4):1082–1084.

Drakopoulos, M., Snigirev, A., Snigireva, I., and Schilling, J. (2005). X-ray high-resolution diffraction using refractive lenses. *Applied Physics Letters*, 86(1):014102.

Erell, E., Etzion, Y., Carlstrom, N., Sandberg, M., Molina, J., Maestre, I., Maldonado, E., Leal, V., and Gutschker, O. (2004). "Solvent": development of a reversible solar- screen glazing system. *Energy and Buildings*, 36(5):467–480.

Ha, P. T. H. (2016). A concept for energy-efficient high-rise buildings in Hanoi and a calculation method for building energy efficiency factor. *Procedia engineering*, 142:154–160.

Han, Y., Hamada, M., Chang, I.-Y., Hyeon-Deuk, K., Kobori, Y., and Kobayashi, Y. (2021). Fast t-type photochromism of colloidal cu-doped ZnS nanocrystals. *Journal of the American Chemical Society*, 143(5):2239–2249.

Hassouneh, K., Alshboul, A., and Al-Salaymeh, A. (2010). Influence of windows on the energy balance of apartment buildings in Amman. *Energy Conversion and Management*, 51(8):1583–1591.

He, Y., Fu, J., and Zhao, Y. (2014). Oblique angle deposition and its applications in plasmonics. *Frontiers of Physics*, 9(1):47–59.

Hossain, M., Drmosh, Q., Yamani, Z., and Tabet, N. (2014). Silver nanoparticles on zinc oxide thin film: An insight in fabrication and characterization. In *IOP Conference Series: Materials Science and Engineering*, volume 64, page 012018. IOP Publishing.

Jolly Bose, R., Vinod Kumar, R., Sudheer, S., Reddy, V., Ganesan, V., and Mahadevan Pillai, V. (2012). Effect of silver incorporation in phase formation and band gap tuning of tungsten oxide thin films. *Journal of Applied Physics*, 112(11):114311.

Kapsis, K. and Athienitis, A. K. (2015). A study of the potential benefits of semi-transparent photovoltaics in commercial buildings. *Solar Energy*, 115:120–132.

Kavei, G. and Nikbin, S. (2015). Substrate temperature effect on the nanoscale multilayer ZnS/Ag/ZnS for heat mirror application. *Materials Science-Poland*, 33(4):760–766.

Kreibig, U. and Vollmer, M. (2013). Optical properties of metal clusters, volume 25. Springer Science & Business Media.

Lee, G. J. and Wu, J. J. (2017). Recent developments in ZnS photocatalysts from synthesis to photocatalytic applications- a review. *Powder technology*, 318:8–22.

Lintymer, J., Gavoille, J., Martin, N., and Takadoum, J. (2003). Glancing angle deposition to modify microstructure and properties of sputter deposited chromium thin films. *Surface and Coatings Technology*, 174:316–323.

Macleod, A. (2010). Oblique incidence and dielectric-coated metals. *Bulletin*, pages 24–29.

Morton, S. M., Silverstein, D. W., and Jensen, L. (2011). Theoretical studies of plasmonics using electronic structure methods. *Chemical reviews*, 111(6):3962–3994.

Pan, Y., Fan, Y., and Niu, J. (2020). Optical properties of ultrathin silver films deposited by thermal evaporation and its application in optical filters. *Infrared Physics & Technology*, 104:103123.

Pandey, R., Angadi, B., Kim, S. K., Choi, J.W., Hwang, D. K., and Choi, W. K. (2014). Fabrication and surface plasmon coupling studies on the dielectric/ag structure for transparent conducting electrode applications. *Optical Materials Express*, 4(10):2078–2089.

Pedrosa, P., Ferreira, A., Cote, J.-M., Martin, N., Yazdi, M. A. P., Billard, A., Lanceros-Mendez, S., and Vaz, F. (2017). Influence of the sputtering pressure on the morphological features and electrical resistivity anisotropy of nanostructured titanium films. *Applied Surface Science*, 420:681– 690.

Priyadharsini, N., Elango, M., Vairam, S., Venkatachalam, T., and Thamilselvan, M. (2016). Effect of temperature and PH on structural, optical and electrical properties of Ni doped ZnSe nanoparticles. *Optik*, 127(19):7543–7549.

Rahchamani, S. Z., Dizaji, H. R., and Ehsani, M. H. (2015). Study of structural and optical properties of zns zigzag nanostructured thin films. *Applied Surface Science*, 356:1096–1104.

Rahmani, M. B., Keshmiri, S.-H., Shafiei, M., Latham, K., Wlodarski, W., du Plessis, J., and Kalantar-Zadeh, K. (2009). Transition from n-to p-type of spray pyrolysis deposited Cu doped ZnO thin films for no2 sensing. *Sensor Letters*, 7(4):621–628.

Sinha, M., Mukherjee, S., Pathak, B., Paul, R., and Barhai, P. (2006). Effect of deposition process parameters on resistivity of metal and alloy films deposited using anodic vacuum arc technique. *Thin Solid Films*, 515(4):1753–1757.

Sivaramakrishnan, K. and Alford, T. (2009). Metallic conductivity and the role of copper in ZnO/Cu/ZnO thin films for flexible electronics. *Applied Physics Letters*, 94(5):052104.

Sobahan, K., Park, Y. J., and Hwangbo, C. K. (2009). Effect of deposition angle on the optical and the structural properties of Ta_2O_5 thin films fabricated by using glancing angle deposition. *Journal of the Korean Physical Society*, 55(3):1272–1277.

Taschuk, M. T., Hawkeye, M. M., and Brett, M. J. (2010). Glancing angle deposition. *In Handbook of Deposition Technologies for Films and Coatings*, pages 621–678. Elsevier.

Usami, A. and Kawasaki, N. (2012). Modeling of solar spectral irradiance data from cloudless to overcast skies. *Japanese Journal of Applied Physics*, 51(10S):10NF06.

Venugopal, N. and Mitra, A. (2013). Optical transparency of zno thin film using localized surface plasmons of Ag nanoislands. *Optical Materials*, 35(7):1467–1476.

Vrakatseli, V. E., Kalarakis, A. N., Kalampounias, A. G., Amanatides, E. K., and Mataras, D. S. (2018). Glancing angle deposition effect on structure and light-induced wettability of RF-sputtered TiO_2 thin films. *Micromachines*, 9(8):389.

Wang, L., Xu, X., Cheng, Q., Dou, S. X., & Du, Y. (2021). Near-Infrared-Driven Photocatalysts: *Design, Construction, and Applications*. Small, 17(9), 1904107.

Wang, Y., Runnerstrom, E. L., and Milliron, D. J. (2016). Switchable materials for smart windows. *Annual review of chemical and biomolecular engineering*, 7:283–304.

Xiao, X., Dong, G., Xu, C., He, H., Qi, H., Fan, Z., and Shao, J. (2008). Structure and optical properties of Nb_2O_5 sculptured thin films by glancing angle deposition. *Applied Surface Science*, 255(5):2192–2195.

Ye, Y., Loh, J. Y., Flood, A., Fang, C. Y., Chang, J., Zhao, R., Brodersen, P., and Kherani, N. P. (2019). Plasmonics of diffused silver nanoparticles in silver/nitride optical thin films. *Scientific reports*, 9(1):1–11

Yildiz, A., Cansizoglu, H., Turkoz, M., Abdulrahman, R., Al- Hilo, A., Cansizoglu, M., Demirkan, T., and Karabacak, T. (2015). Glancing angle deposited Al-doped ZnO nanostructures with different structural and optical properties. *Thin solid films*, 589:764–769.

Zahiri, S. and Altan, H. (2016). The effect of passive design strategies on thermal performance of female secondary school buildings during warm season in a hot and dry climate. *Frontiers in built environment*, 2:3.